공학석사학위논문

Visualization of Cryogenic Liquid Nitrogen Jet using Raman Scattering

라만 산란을 이용한 극저온 액체 질소 제트 분무의 가시화

2015 년 8 월

서울대학교 대학원

기계항공공학부

김 해 솔

Visualization of Cryogenic Liquid Nitrogen Jet using Raman Scattering

2015년

김해솔

↑
2.5cm
↓

↑
↓

Abstract

Visualization of Cryogenic Liquid Nitrogen Jet using Raman Scattering

Haisol Kim

Department of Mechanical and Aerospace Engineering

The Graduate School

Seoul National University

An investigation on injection characteristics simulating real rocket combustion chamber conditions has been carried on through this research. Liquid nitrogen was used for simulating cryogenic rocket propellants, and injection experiments were conducted inside a high pressure chamber to form various pressure conditions. To overcome the limitation of short visualization window and to have quantified result, laser induced Raman scattering technique has been applied to the investigation of the cryogenic flow. An emission of Raman scattering and a proper combination of filters have been verified prior to the main experiments. The filter set was formed to block the incident beam wavelength with an amount of 10^{-16}. Breakdown-inducing laser power was also measured and the power was limited not to form a plasma.

The main experiments were conducted with varying ambient pressure conditions from 20 bar to 50 bar, which is from subcritical to supercritical condition of nitrogen. Raman scattering signal images from the nitrogen jet have been depicted by ICCD camera, and the images went through a series of reduction process consist of background subtraction, Gaussian beam profile effect normalization, and beam attenuation effect compensation. The refined data was quantified into a density map, and analyzed from the various viewpoint.

The density maps showed the distribution of nitrogen jet after the injection in absolute numbers. Moreover, with focusing on axially 0.5d position, the trend of injection density change with the ambient pressure increase has been observed, which had increased under the subcritical conditions but had converged under the supercritical conditions. The analysis on normalized properties also has been conducted. Axially normalized data showed the trend of faster dissipation along the axis when the ambient pressure increases under the supercritical conditions. Radially normalized data was used for the jet similarity study, and it showed larger deviation under the subcritical conditions. Ramanographs were drawn for the ease of understanding density distribution in two dimension, and compared with unfiltered scattering signal image, which showed the advantage of applying Raman scattering technique.

Keywords: Raman scattering, Laser diagnostics, Jet injector, Cryogenic, Supercritical, Liquid nitrogen

Student Number: 2013-23063

Contents

List of Tables

List of Figures

Chapter 1 INTRODUCTION

1.1 Cryogenic injection and supercritical fluid

In real rocket engine, cryogenic fluid such as liquid hydrogen and liquid oxygen is often used as a propellant due to its high volume efficiency and good energy density. When the cryogenic propellant is injected into a combustion chamber of a rocket engine, a large amount of pressure is built up in the chamber due to the vaporization of the propellant, the combustion process, and the existence of a nozzle. In order to inject the propellant into the combustion chamber, the pressure in the feeding line or in a turbo pump needs to be higher, and therefore, the system forms supercritical condition which makes the propellant into a supercritical fluid.

$$\frac{\mathrm{P}_1}{\gamma} + \frac{v_1^2}{2g} + z_1 = \frac{\mathrm{P}_2}{\gamma} + \frac{v_2^2}{2g} + z_2 \tag{1.1}$$

From the Bernoulli's equation above, where subscripts 1 and 2 indicate inside and outside the chamber respectively, higher chamber pressure results in higher exit velocity, which means the better engine performance. However, at the same time, the maximum chamber pressure is limited by material characteristics and propellant feeding system capability such as turbo pump specification. For these reasons, actual chamber pressure condition varies depending on the countries and the type of rockets.

Table 1.1 Chamber pressure design of several rocket engines*

	Engine designation			
	AJ-10-1181	RS-27	RCS	LE-7 (Japan)
Application	Delta II second stage	Delta II space launch booster	Attitude control	H-II launcher booster
Vacuum thrust (kN)	43.83	921.15	0.08	1079.13
Chamber pressure (bar)	8.61	39.69	4.82	132.08**

* Data selected from table 8-1 of *Rocket Propulsion Elements*, and units were converted [1].

** Nozzle end stagnation pressure value used instead.

According to table 1.1, even though the amount of pressure is different depending on the purpose of engines, the fact that chamber pressure needs to be higher than, or at least near, the critical condition of cryogenic rocket propellants is true for high thrust main engines to have better performance.

The aforementioned statements conclude that the condition in the real rocket engine is clearly different from the room temperature and pressure, so the necessity on the injection study simulating the real rocket chamber condition has risen. In this study, cryogenic liquid nitrogen was injected as a simulant of cryogenic propellant, and the injection experiment was carried on inside the high pressure chamber to simulate the combustion chamber pressure.

1.2 Overview of previous works

Nitrogen behaves as supercritical fluid over the pressure of 3.40 MPa (34 bar) and the temperature of 126.19 K. To build up the pressure more than 30 times of the atmosphere, high pressure chamber facility is necessary. Moreover, cryogenic fluid feeding system is also very complicated, so this kind of complex injection characteristic study was not easy for researchers to study. Nevertheless, there have been several research groups worked on this research theme.

Cho et al. from Seoul National University tried to investigate the dynamic characteristic of cryogenic swirl flow under the supercritical condition [2]. They used liquid nitrogen as an oxidizer simulant, and analyzed spray characteristics using high speed images of the swirl flow. They depicted sinusoidal wave shape on the surface of swirl flow from the images, and computed the repetition rate using linear laser beam transmitting the spray. However, in their experiments, drastic density change of the injected liquid nitrogen resulted in high optical density, so temporal visualization window was too short to be analyzed quantitatively (less than 1 second). From the result of their research, together with the direct photography result presented at figure 1.1, a necessity of proper technique for a quantitative research was risen.

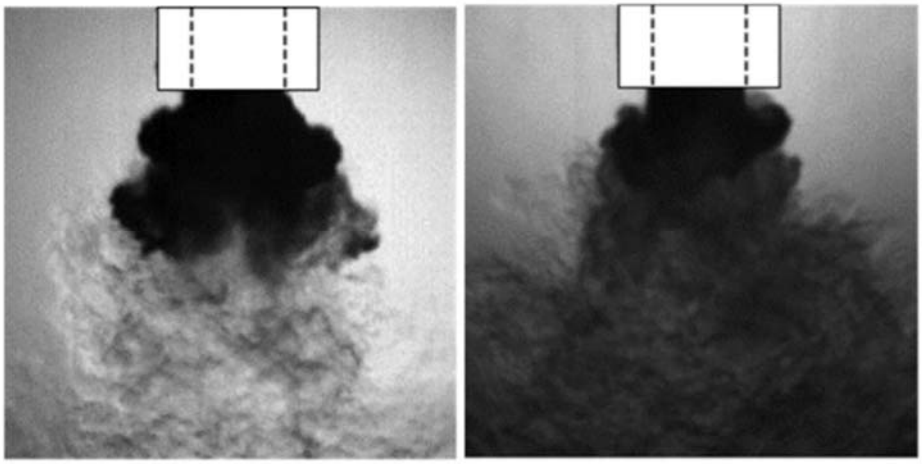

Figure 1.1 Fuzziness of cryogenic nitrogen injection region [2]

Deeper investigation on the technique which can be applied to the supercritical fluid injection characteristic analysis led to the research cases conducted by German Aerospace Center (DLR) [3, 4] and Air Force Research Laboratory (AFRL) [5, 6] in late 1990s and early 2000s. Both research groups had an objective of investigating cryogenic nitrogen flow characteristics injected by shear coaxial jet injector, quantitatively. Even though the exact experimental set up was not the same, both groups applied Raman diagnostics technique to map the density distribution of the injection region. For the case of DLR research group [4], two ICCD cameras were set at the data acquisition part, and the difference between unfiltered image and filtered image was computed to acquire the pure Raman scattering signal (figure 1.2). On the other hand, research group of AFRL used several combinations of filter set to perfectly block the incident beam wavelength and pass the Raman scattering signal [5, 6] (figure 1.3).

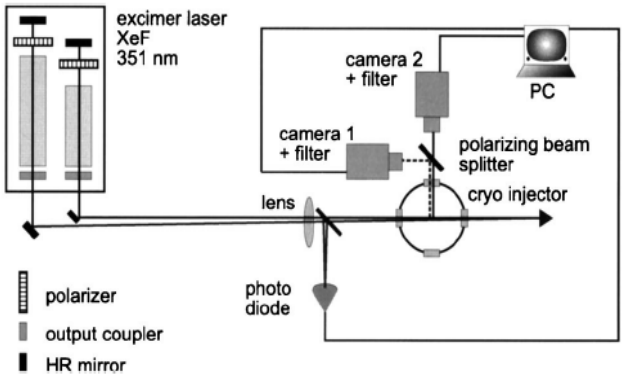

Figure 1.2 Experimental set up of previous research (DLR [4])

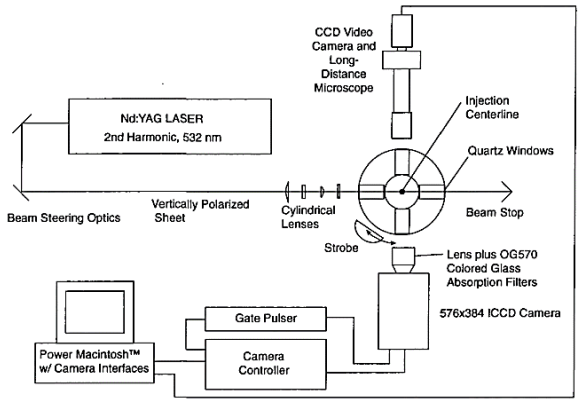

Figure 1.3 Experimental set up of previous research (AFRL [5])

Even though the previous research results showed the density distribution of injected nitrogen jet under the supercritical conditions, the result also has a limitation that not various pressure conditions were considered for the experiments. Experiments were conducted under only one or two pressure cases of subcritical and supercritical conditions each. Therefore, investigating the trend of injection characteristic with pressure change under subcritical to supercritical condition was not much analyzed.

In this study, the efforts on experiments made by previous research groups were referred, and injection characteristics of cryogenic nitrogen jet was investigated using Raman diagnostics technique from the viewpoint of its tendency with pressure condition change.

1.3 Raman scattering and its application

Raman scattering is an inelastic scattering of light which was predicted by C. V. Raman (1922) and Adolf Smekal (1923), and later discovered by C. V. Raman in 1928 [7]. When an incident light is investigated into a test section where some test molecules are distributed, various kinds of scattered photons are emitted and also fluorescence occurs depending on the conditions. Dominant phenomenon in the scattering is that scattered photons have the same energy as photons from the incident light, however some minor photons show either smaller or larger energy which is expressed in wavelength change and this is called as Raman scattering (Figure 1.4).

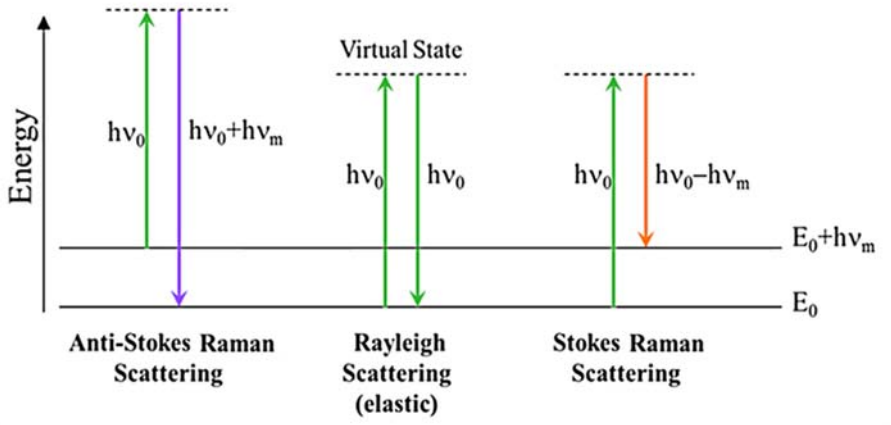

Figure 1.4 Jablonski diagram of Raman scattering

In terms of Stokes Raman scattering, molecules at ground state are excited by an incident beam to a virtual state of which the level is as high as the energy of

the incident photon. An energy difference between the excited state of the molecule and its 1st excited vibrational state is emitted, and naturally the wavelength of the emitted scattering signal is longer than the incident beam.

Despite the defect that the signal intensity of the Raman scattering is too small comparing with the incident beam and elastic scattering signal intensity, a big advantage of the Raman scattering is that no tunable light source is required, unlike fluorescence technique. As mentioned above, the wavelength of the Raman scattering signal is determined with the relation between the characteristics of the incident beam and the molecule. Wavelength change of nitrogen molecule for Raman scattering is already experimented and known as 2331 cm^{-1} in wavenumber [8]. For example, assuming 532 nm (Nd:YAG laser 2nd harmonic) laser beam is used as a light source, wavelength of the stokes Raman scattering signal, $\lambda_{R_{Stokes}}$, becomes 607.31 nm according to the following equation 1.2 (plus sign for computing anti-Stokes Raman scattering signal).

$$\frac{1}{532\,nm} \pm 2331 \times 10^{-7}\ \mathrm{nm}^{-1} = \frac{1}{\lambda_R} \tag{1.2}$$

The intensity of Raman scattering signal, *I*, is expressed as equation 1.3,

$$I = \alpha\sigma(\rho)\rho E \tag{1.3}$$

where α is the experimental coefficient, σ is Raman scattering cross section, ρ is species density, and *E* is the incident beam intensity. Equation 1.3 shows that Raman scattering cross section is also a function of density, but its

dependency under the supercritical condition was not studied enough, and therefore, Raman scattering cross section was assumed to be constant with referring the previous study [3]. As a result, equation 1.3 can be reduced into equation 1.4, which means that when a Raman scattering signal intensity (I_R) of the density-known (ρ_R) region is acquired, density value of any region can be calculated from the intensity of Raman scattering signal based on the linear relation.

$$\frac{I_R}{\rho_R} = \frac{I}{\rho} \tag{1.4}$$

Chapter 2 EXPERIMENT APPARATUS AND METHOD

2.1 Jet injector and high pressure chamber

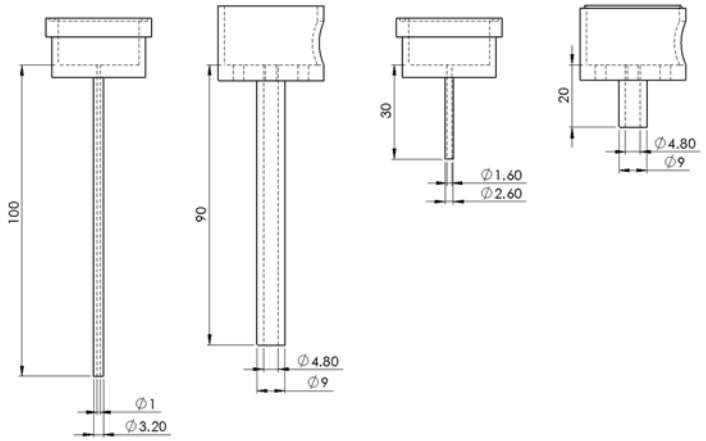

Type	A	B	C	D
l/d	100	18.75	18.75	4.17

Figure 2.1 Designed injectors with length to diameter ratio

For this study, several types of injectors have been designed and made. Basically, all the injectors were designed to be usable as both single jet injector and shear-coaxial injector with assembling the parts. For the experiment apparatus of Chehroudi et al. [6], cooling jacket around the injector was devised, therefore cryogenic fluid could be injected in to the chamber in liquid phase. However, there was a limitation for the test facility in this research, and the injector was designed to be naturally cooled down by primary flowing fluid at the beginning of each experiment cases. Still there was an uncertainty on the heat transfer rate between

the cryogenic fluid and relatively hot injector, so the determination of length and thickness of the injectors depended on the experience and trial and error method to some extent.

Among the designed injectors arranged in Figure 2.1, model B was selected as the most adequate one for this study. As the maximum length was bound as 100 mm, larger diameter design caused smaller l/d ratio which would affect the development of the flow. At the same time, diameter had a lower limit due to the mass flow rate requirement, which would guarantee the liquid phase injection.

The l/d value of 18.75 was selected considering not just a theoretical standpoint but also the ease of manufacturing. According to Schlichting [9], fully developed flow could be achieved with l/d around 20, therefore this injector design was expected to show a transient phenomenon.

For this research, high pressure chamber facility already built at Rocket Propulsion Lab of Seoul National University was used (Figure 2.2). Its inner diameter is 50 cm, but visualization windows installed at each side of the chamber had a length of 30 cm, which resulted in long distance between the injector and the camera sensor more than 60 cm. This long distance had a negative effect on capturing Raman signal which is very week, and it reduced signal to noise ratio.

The chamber was designed to work under the pressure condition of as high as 60 bar. Considering that the critical pressure of nitrogen is 34 bar, the specification of the chamber was enough to make a supercritical condition.

Two sets of pressure sensor and thermocouple were installed to measure the properties inside the chamber and the injector, respectively.

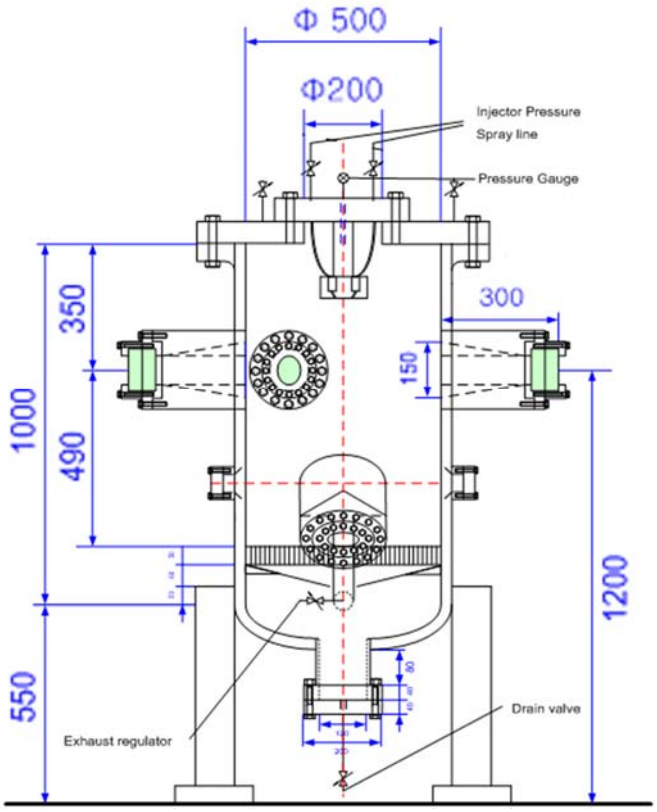

Figure 2.2 Schematics of high pressure chamber

2.2 Probe laser, ICCD camera, and optical elements

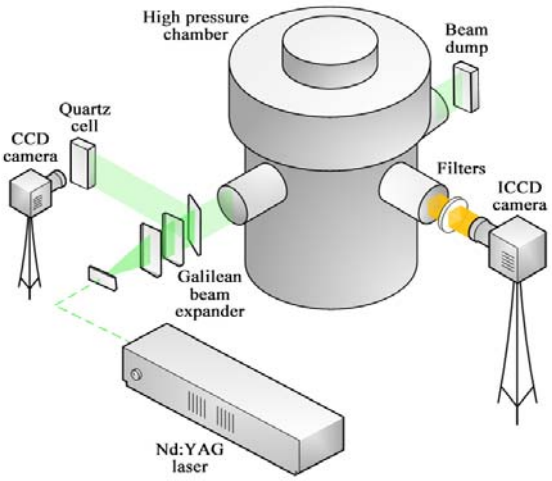

Figure 2.3 Schematics of experimental apparatus

Overall experimental setting has been drawn in Figure 2.3. To induce a Raman scattering signal from injected liquid nitrogen, Continuum Surelite II PIV laser was selected as a light source in this study. It is 10 Hz pulse laser, and the wavelength of the beam was set as 532 nm with frequency doubling. Under this condition, maximum power was measured as 3.1 W, therefore each pulse had 310 mJ at maximum. Even though Raman scattering signal intensity is proportional to the incident beam intensity (Equation 1.3), there was an upper limit in power setting, due to the break down phenomenon, and this effect will be discussed in the chapter 3.1 Raman signal verification.

As described in chapter 1, Raman signal has very low intensity comparing with incident beam or Rayleigh scattering signal. Therefore, Intensified CCD (ICCD)

camera with a set of filters was used for capturing the Raman scattering signal. The model was PI-MAX from Princeton Instruments, and a specification chart provided by the company showed the quantum efficiency around 12 %.

Figure 2.4 Surelite II PIV laser and PI-MAX ICCD camera

In front of the ICCD camera, a set of filters were installed to block the stray light while passing the band of Raman scattering signal. Signal intensity of the Raman scattering was not easy to estimate, as the experimental coefficient couldn't be computed from the theory, therefore the experiment setup of previous research cases has been investigated and listed in Table 2.1.

Table 2.1 Filter set specifications from previous researches

Previous research cases	No. of filters	Transmittance at laser wavelength	Transmittance at Raman band
Woodward and Talley [5]	1	10^{-5*}	not specified
Oschwald et al. [3, 10]	2	10^{-12}	not specified
Chehroudi et al. [6, 11]	3	10^{-15}	0.23

* It was stated that the light was attenuated by order of 50, but the specification shows order of 5

From the previous research cases, required blockage rate for the incident beam wavelength has been estimated, and several high pass filters and band pass filters were prepared. The candidate filters are listed in the following Table 2.2.

Table 2.2 Filters to block the incident beam wavelength and to pass Raman signal

Model (manufacturer)	Type	Qty.	Transmittance at laser wavelength	Transmittance at Raman band
600FS20-50 (Andover)	600 nm band pass	2	$10^{-4.5} \times 10^{-4.5}$	0.7 × 0.7
550FG05-25 (Andover)	550 nm high pass	1	10^{-3}	0.9
570FG05-25 (Andover)	570 nm high pass	1	10^{-4}	0.9
YIF-BA575-625S (OptoSigma)	600 nm band pass	2	$10^{-4} \times 10^{-4}$	0.9 × 0.9

Among the filters listed in Table 2.2, proper combination has been chosen from a liquid nitrogen dropping test with using a monochromator. Detailed process would be explained in chapter 3.1, and as a result, two band pass filters (600FS20-50) and two high pass filters (550FG05-25, 570FG05-25) from Andover Corporation were installed in combination for this study. The overall blockage rate was 10^{-16} at 532 nm wavelength band, and the transmittance of 607 nm Raman band was 0.24.

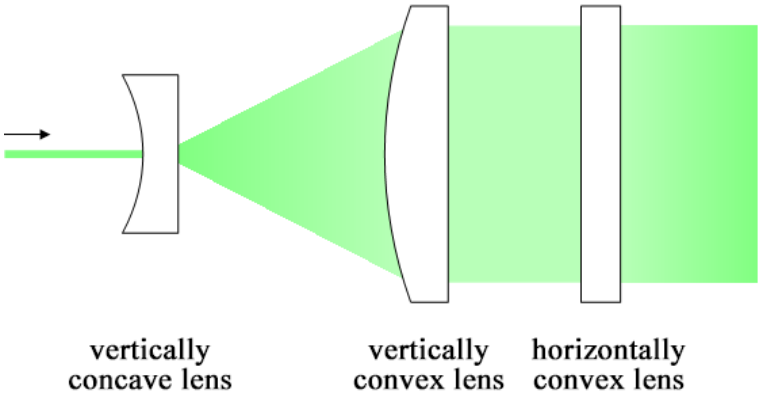

Figure 2.5 Schematics of laser sheet shaping optics

To investigate the injection area in two dimension, Galilean beam expander has been set using cylindrical lenses to form a laser sheet (Figure 2.5). Firstly, a cylindrical concave lens which has -40 mm focal length was used for stretching the linear beam vertically. A cylindrical convex lens of 800 mm focal length was at next to make the beam parallel. At last, a cylindrical convex lens was located to converge the beam horizontally, so that the sheet beam becomes thin enough at the injection area.

Due to the difficulty in measuring the energy of laser sheet from the stretched shape, all the values of incident laser power stated from now on is the intensity measured at right before the Galilean beam expander.

2.3 Experiment condition

In this study, the main experimental parameter is the chamber pressure. With a critical pressure of nitrogen (34 bar) as a criterion, subcritical conditions (20, 25, 30 bar) and supercritical conditions (35, 40, 45, 50 bar) were selected as chamber pressure conditions. An injection pressure difference has been maintained as 0.75 bar with controlling the pressure of the chamber and the liquid nitrogen run tank. Therefore the injected liquid nitrogen experiences property change along the arrow lines indicated in figure 2.6 for each pressure conditions.

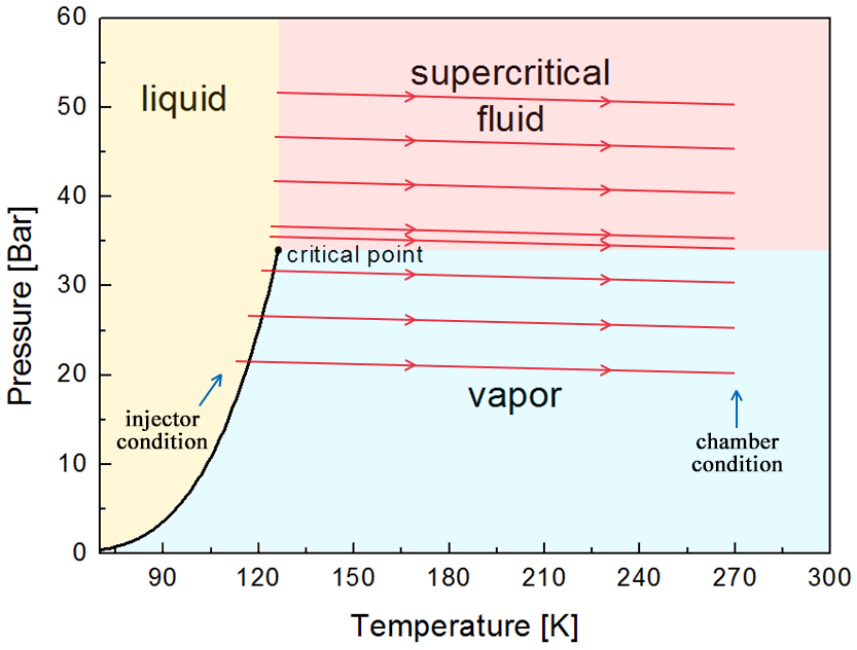

Figure 2.6 Property change of the injected liquid nitrogen for each experiment cases (based on NIST chemical property data)

The Raman scattering signal of the injected nitrogen was recorded only when the injector cooled down enough, and the temperature of the injector changed slightly from 113 K to 127 K with increasing the chamber pressure. The chamber temperature condition was controlled as 270 K with waiting after each experiment cases for the chamber to be warmed up enough.

Laser specification is also an important parameter to be controlled. The pulse energy was limited as 220 mJ to avoid the break down phenomenon and plasma formation. Using the Galilean beam expander, the laser beam was stretched vertically, and only the central part of it was used to reduce the intensity variation caused from the Gaussian beam profile (refer the part 3.2.2). As a result, the height of the laser sheet was 40.5 mm at the injection area, and the width was set as 1.1 mm. The laser sheet width could be thinner, but the break down could occur due to the focused energy.

The data acquisition condition of Raman scattering signal has been mainly determined by the specification of the ICCD camera. The maximum resolution of the ICCD camera was 1024 × 1024 pixels, but 2 × 2 pixels were grouped into one cell to increase the sensitivity, which resulted in the resolution of 512 × 512 pixels. The gate width of each shots was set as 30 ns for the laser pulse of 8 ns long to be placed in between. With a shot trigger rate being synchronized with the laser pulses, which is 10 Hz, data delivery rate of the ICCD was not fast enough to proceed every single shot it takes. Moreover, the Raman scattering signal was too weak to be clearly recognized from the background noise. Not to miss the data from the slow data process rate, and to increase the signal to noise ratio (SNR) of the Raman scattering signal, on-CCD accumulation function of

the ICCD camera was used. 5 shots were accumulated on the CCD and transferred to the computer at once, so that a signal data file was recorded each 0.5 second and SNR naturally increased about 5 times higher. Due to this setting, instantaneous distribution of injected liquid nitrogen couldn't be depicted, but average profiles with stronger intensity could be acquired.

Table 2.3 Experiment condition

Injection	Ambient pressure [bar]	20, 25, 30, 34*, 35, 40, 45, 50
	Injection pressure difference [bar]	0.75
	Manifold temperature [K]	113 ~ 127
	Chamber temperature [K]	270 ~ 280
Laser sheet	Pulse energy [mJ/pulse]	220
	Height [mm]	40.5
	Width [mm]	1.1
Data acquisition	Resolution [pixel x pixel]	512 x 512
	Gate width [ns]	30
	Accumulation	5 images

* Critical pressure of nitrogen

Chapter 3 RESULTS AND DISCUSSION

3.1 Raman signal verification

3.1.1 Filter blocking test

Due to the weak intensity, it was impossible to record the Raman scattering signal in two dimensional data plane while verifying the signal wavelength with monochromator at the same time. Therefore, only ICCD camera could be used for the high pressure chamber experiment, and it needed to be guaranteed that the filter set, which would be installed in front of the camera, could perfectly block 532 nm incident beam wavelength and passes 607 nm Raman signal wavelength.

Prior to the main experiment in the chamber, verification of Raman scattering signal emission and filter performance test were conducted. High pressure chamber facility was not easy to do simple experiments with, so small test rig to conduct liquid nitrogen drop test was designed and set as described in figure 3.1.

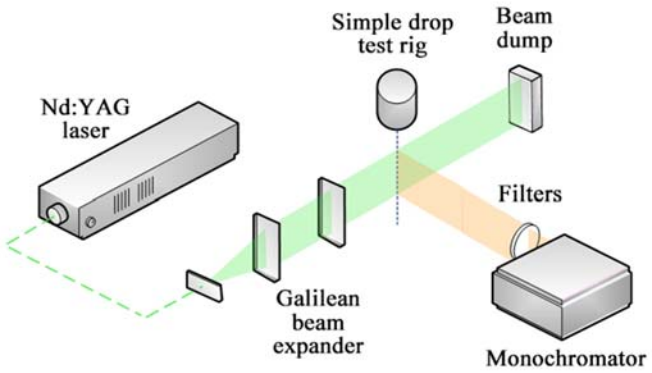

Figure 3.1 Schematics of liquid nitrogen drop test facility

A monochromator was installed to analyze the wavelength of the emitted signal, and several types of filter combination have been tested to analyze the blockage rate of 532 nm incident beam wavelength. Liquid nitrogen was poured into a cup-like reservoir which has a hole at the bottom. Nitrogen droplets were formed, and laser induced scattering signals including Raman scattering were detected.

The first test resulted that when there was no filter installed in front of the monochromator, where the ICCD camera mounted, the scattering signal of 532 nm was not able to be recorded due to its high intensity which would damage the CCD; saturation intensity of the CCD is 65536. Therefore, two Andover band pass filters were located and the data was recorded. Figure 3.2 shows the spectrum analysis of scattering signal near 607 nm, and figure 3.3 is around 532 nm wavelength.

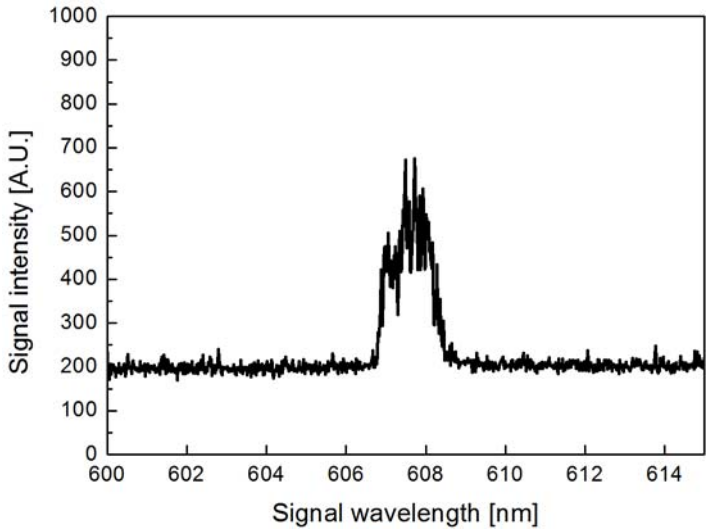

Figure 3.2 Spectrum analysis of scattering signal at 607 nm

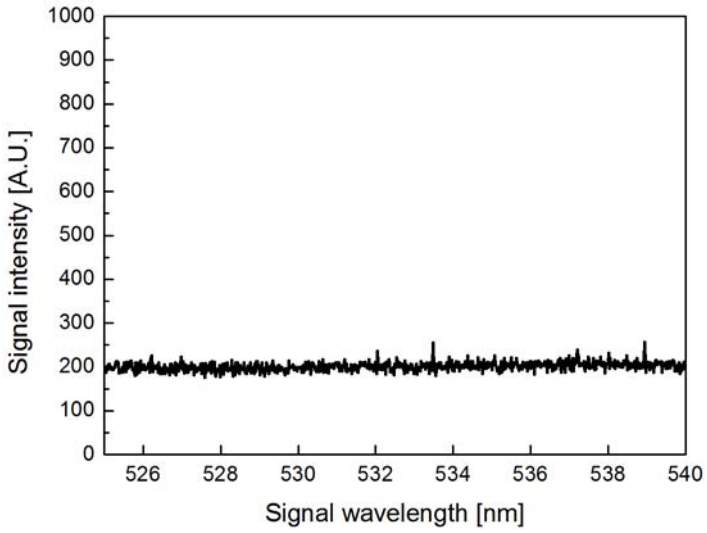

Figure 3.3 Spectrum analysis of scattering signal at 532 nm

The blockage rate of the two Andover band pass filters was 10^{-9} at 532 nm wavelength, and it passed around 50 % of 607 nm Raman signal. The resulted signal acquisition data given in figure 3.2 and 3.3 shows that the combination of two filters are sufficient to acquire Raman scattering signal. However, in the high pressure chamber experiment, two more high pass filters were added to give a margin in blockage rate.

3.1.2 Plasma inhibition

In addition to the perfect blocking of the signal which has an incident beam wavelength, inhibiting the plasma formation was also an important process to acquire Raman scattering signal from the fluid. During the filter blockage test of this study, plasma formation was detected and recorded. The test set up was the same as figure 3.1, but the horizontally focused region of the laser beam was right

below the injector. When plasma was formed from a liquid nitrogen droplet, dark orange colored light with very high intensity was emitted, which could even observed with bare eyes. The formation of plasma was depicted with DSLR camera (figure 3.4) through the filter set combined in the previous chapter.

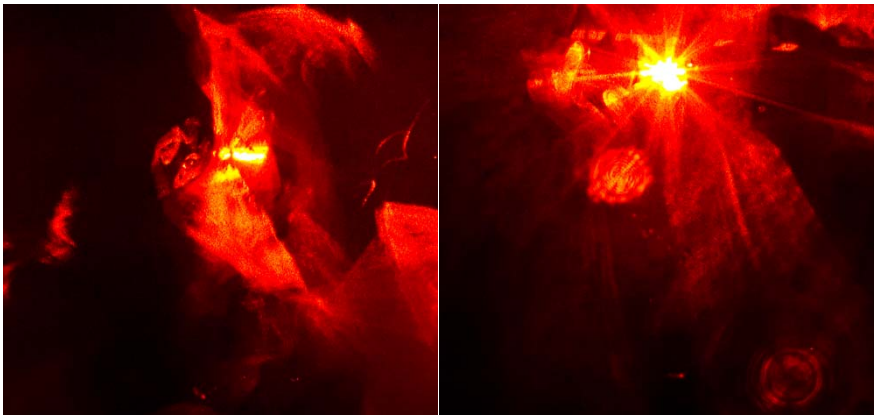

Figure 3.4 Plasma formation from liquid nitrogen droplet

As can be seen from figure 3.4, plasma was formed when the central part of the laser sheet meets a liquid droplet. The light was emitted in radial shape. Moreover, when the plasma is formed, it had its own sound which is similar to what we can here when the laser beam hits and burns certain object.

To investigate the wavelength of the signal from the plasma, monochromator was used. The result showed the wavelength of 607 nm, and it was exactly same as the Raman band of nitrogen. To analyze this phenomenon, laser induced breakdown spectroscopy (LIBS) has been investigated, but a clear explanation on the relation between the wavelength of Raman signal and continuum was not found, which may require further study.

Due to the high intensity of the signal emitted from the plasma formation, it needed to be inhibited to detect Raman scattering signal. With referring previous research [11], pulse stretching loop, which preserves the total energy while stretching it temporally, was set to inhibit the plasma formation (figure 3.5).

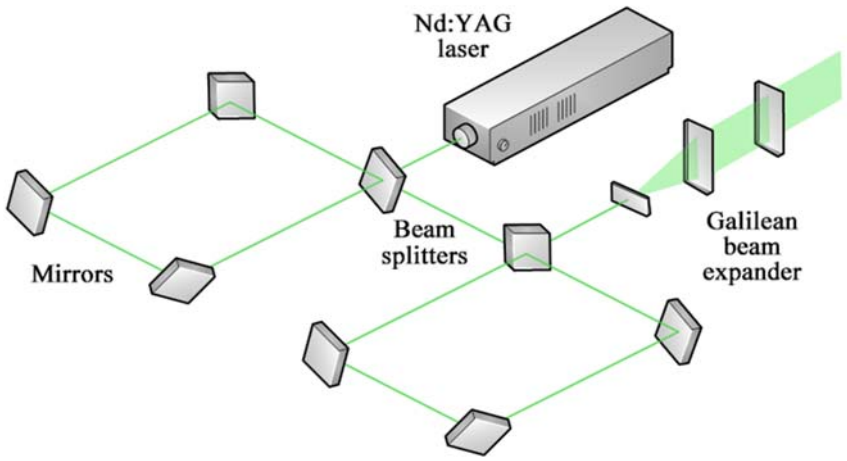

Figure 3.5 Pulse stretcher devised to inhibit the plasma formation

As a result, laser pulse initially 10 ns long has been stretched into 30 ns long in full width half maximum (FWHM) of the energy. However, a loss of the energy while the beam passes two beam splitters and six mirrors was not negligible, and resulted in the final beam power which is just 67 % of the initial one. Not just the power loss from the optical elements, but the delicate alignment was also a problem of the pulse stretcher. Setting all the laser lines to be located in the exact same way was not a simple task, and this deviation also resulted in the energy loss. Naturally, the intensity of Raman scattering became smaller, and therefore, it was not detected by the ICCD camera.

Rather than using pulse stretcher, it was determined to use the original laser beam with decreasing the laser power. Laser power of 2.2 W was found to be the maximum while not generating plasma, under the optical element setting of this study. When the main experiment inside the high pressure chamber was conducted, laser sheet was attenuated due to the quartz window, so the laser power level and horizontally focusing position were modified slightly depending on the experimental condition of each cases.

3.2 Data reduction and quantification

After verifying the emission of Raman scattering signal and the proper beam energy level setting, the main experiment started inside the high pressure chamber using the liquid nitrogen feeding system. The equipment and optical elements were set as figure 2.3. Experiment conditions including chamber pressure and injection pressure difference were set in accordance with the table 2.3, and Raman scattering signal was monitored and recorded simultaneously when liquid nitrogen is injected.

In order to analyze the result quantitatively, the acquired data went through a reduction process. The process is consist of subtracting background, normalizing Gaussian beam profile effect, and compensating the experiment case deviation caused from the attenuation of laser power inside the pressurized chamber.

3.2.1 Background subtraction

Background subtraction is a simple task to eliminated background noise included in the depicted Raman scattering signal. Several background shots were taken, before the laser is investigated into the chamber, and the average of the shots were subtracted from the acquired signal data. This process resulted in making the signal values outside the injection region into near zero.

3.2.2 Beam profile effect normalization

The next step was beam profile effect normalization. Due to the characteristic of laser beam formation, the intensity profile of laser sheet follows Gaussian distribution. To minimize the error caused by the beam intensity difference, the

laser sheet was over expanded and only the central part of the sheet was used. However, still there was the strongest region at the center, and top and bottom part had weaker intensity. Right before the laser sheet goes into the chamber, a beam sampler (Sigma Koki BS4) was located as indicated in figure 2.3 and 5 % of the incident beam was reflected to a quartz cell (NSG precision cell 23ES10). In the quartz cell, Rhodamine 590 solution was filled and illuminated as the laser sheet is investigated. Using Canon 7D DSLR camera, raw images, which have color depth of 14 bit, were captured. The image of illuminated cell and beam intensity profile are shown at figure 3.6.

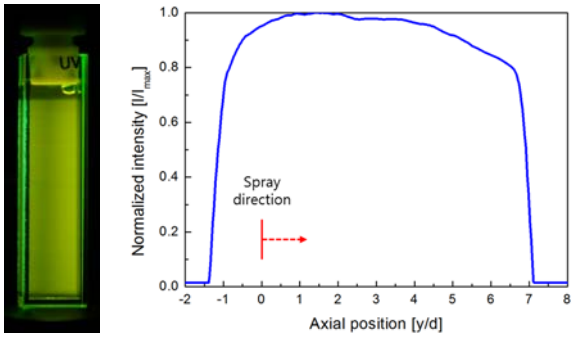

Figure 3.6 Illuminated quartz cell and beam intensity profile

At 0d position, the injector tip was located and liquid nitrogen was injected downward (in axial direction). Naturally, due to the intensity difference, Raman scattering signal at some parts were more amplified than other parts, so the scattering signal intensity values at each axial position were divided by the normalized intensity value of the same position. Through this normalization process, the effect of laser sheet intensity distribution has been corrected.

3.2.3 Beam attenuation effect compensation

The last step of the data reduction process was taking the beam attenuation effect into account. When the beam propagates, it is attenuated due to the optical elements, visualization quartz window, and liquid droplets floating inside the chamber. While the attenuation due to the optical elements and the visualization window was constant, the intensity decrease rate inside the chamber due to the fluids varied with chamber pressure conditions. Some extra experiments were conducted to analyze the attenuation inside the chamber. Liquid nitrogen was injected through the injector for 3 seconds and then stopped. At the moment that the injection stopped, the beam intensity values which began to decrease were recorded, and graphed in figure 3.7.

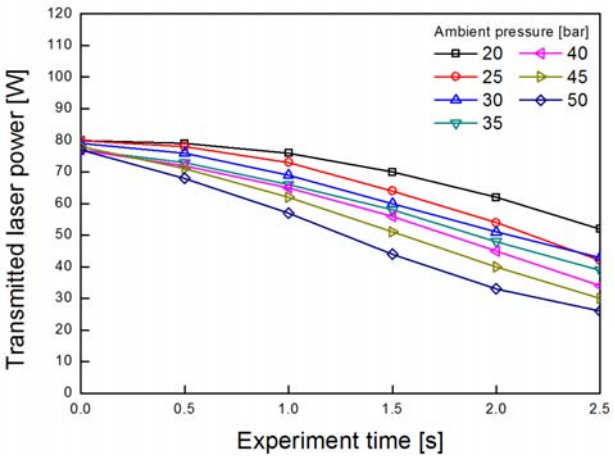

Figure 3.7 Beam attenuation profile with different chamber pressure

Time 0 can be considered as the condition before the injection. Raman scattering signal data depicted at the time of 1 and 1.5 second were taken in this study for the

analysis. Therefore, the average value of the beam intensity data at 1 and 1.5 second were chosen for the correction standard. In accordance with the chamber pressure conditions, the computed factors have been divided to compensate the error caused from the difference of beam attenuation.

3.2.4 Data quantification

Through the series of data reduction process, the acquired Raman scattering signal data has been corrected. Based on this result and equation 1.3, density value of the injected fluid could be quantified. First of all, Raman scattering signal data acquired right before the injection was used as a reference data set. As the chamber was pressurized to different pressure conditions, the Raman scattering signal from the gaseous nitrogen also varied, even though it's weak. Based on this reference data, the relation between the signal intensity and the density of the fluid was graphed in figure 3.8.

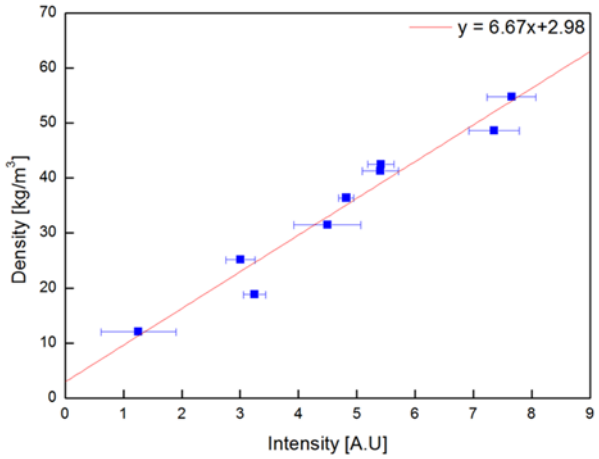

Figure 3.8 Relation between fluid density and Raman signal intensity

With extrapolating the result of figure 3.8, Raman scattering signal intensity values of nitrogen under liquid and supercritical conditions were converted into density value throughout this study. The conversion based on this relation showed the resulting value located in a reasonable region of the nitrogen density, but it still has an error source arise from the accuracy of the extrapolation.

Through the aforementioned data reduction process, except the quantification, depicted Raman scattering signal of the injected nitrogen has been normalized and corrected. As the intensity of the signal is very weak, it has been amplified for the purpose of observing the shape of the flow, and included as figure 3.9.

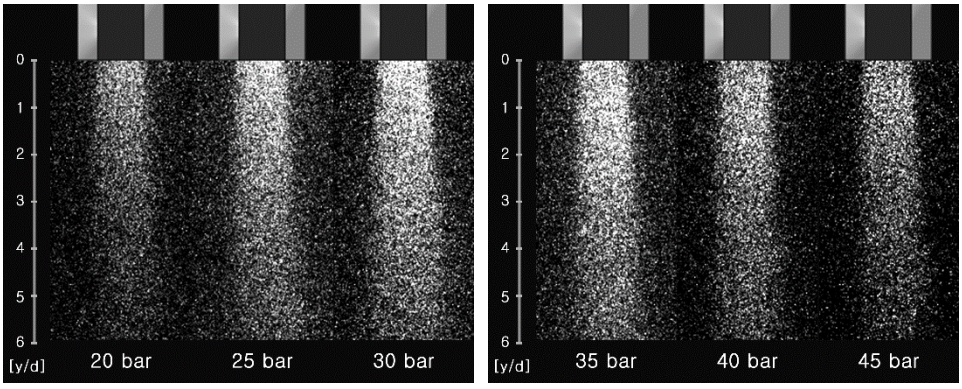

Figure 3.9 Amplified Raman scattering signal after data reduction (subcritical and supercritical condition)

3.3 Density profile analysis

First of all, with converting the signal intensity into the density value, the density distribution profiles of the injected nitrogen under the different pressure conditions were analyzed. For the chamber pressure (ambient pressure) condition from 20 bar to 50 bar, the density distribution at initial region (from 0.5d to 5.5d) of the injection has shown in figure 3.10 and 3.11.

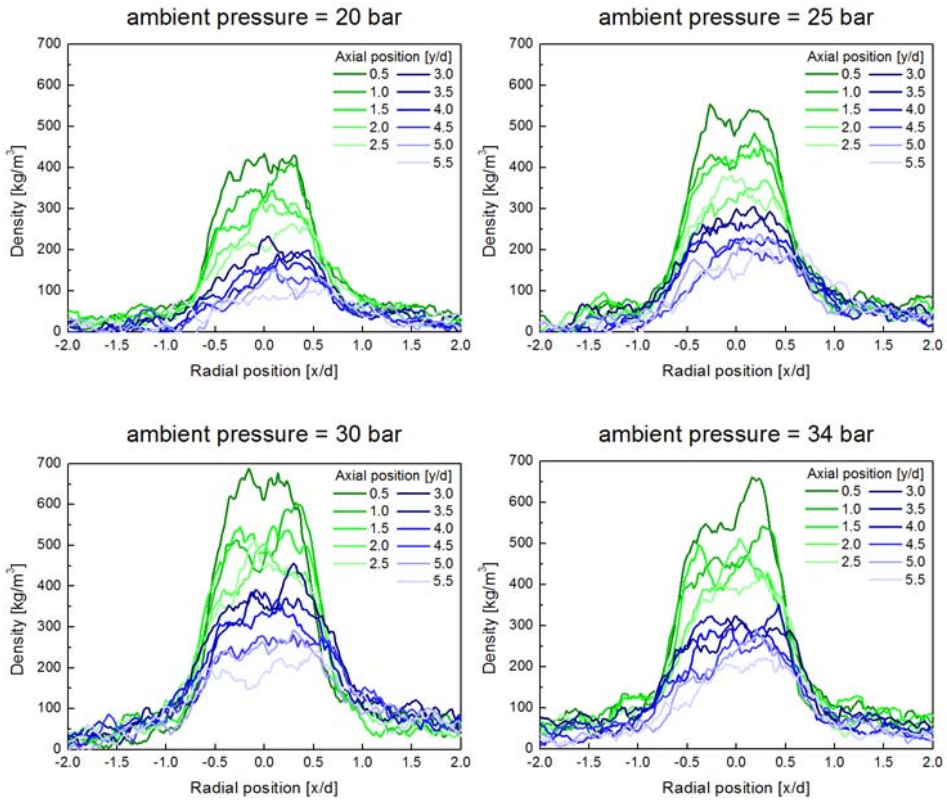

Figure 3.10 Density distribution of injected nitrogen at each axial position under subcritical condition and critical condition (34 bar)

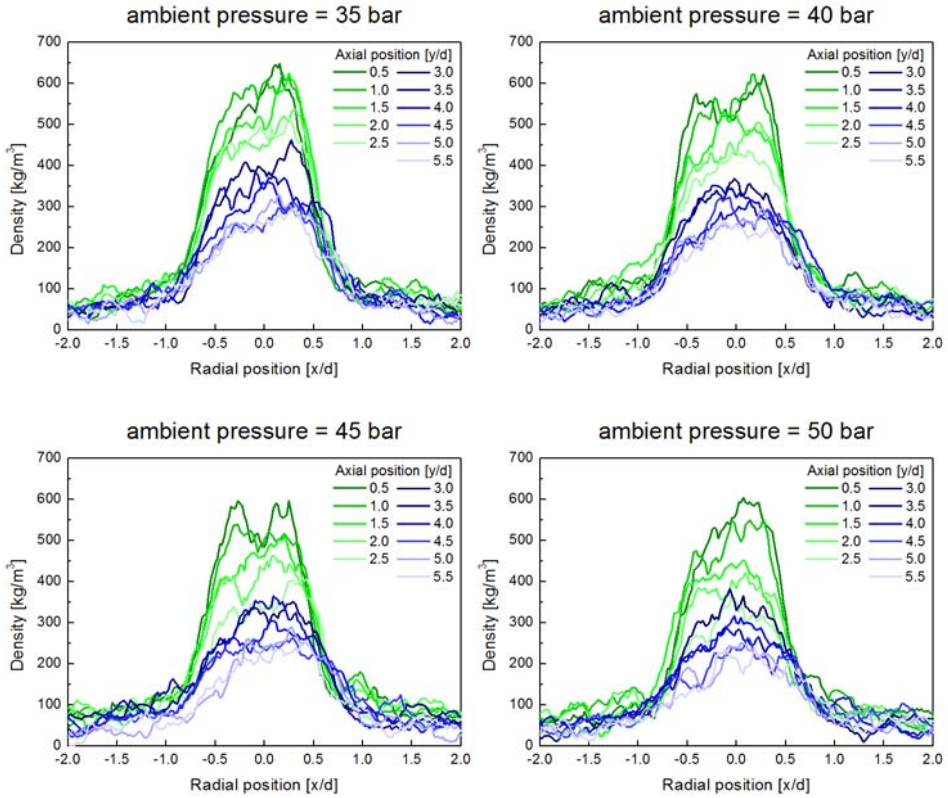

Figure 3.11 Density distribution of injected nitrogen at each axial position under supercritical condition

In figure 3.10 and 3.11, naturally it shows density-decreasing tendency as the injected fluid flows in downward direction (from dark green to light green and then dark blue to light blue in the graph). y/d value from 0.5 to 5.5 can be regarded as an initial region of the injection, so the characteristic of well-preserved width of the flow can be observed from the result of figure 3.10 and 3.11. To compare the density of injected nitrogen right below the injector, under the different ambient pressure conditions, a graph of density distribution at 0.5d location for each cases has been drawn in figure 3.12.

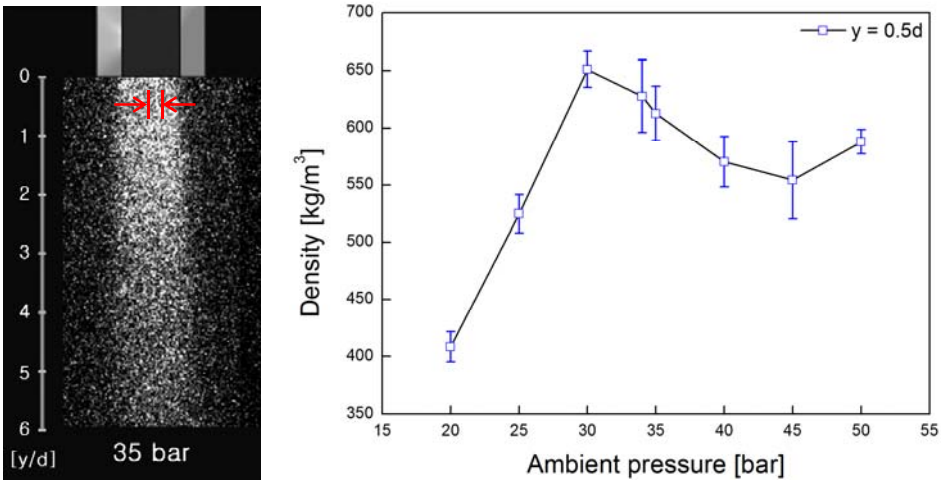

Figure 3.12 Nitrogen density values of central part at axially 0.5d position

The graph of figure 3.12 was drawn with the density data averaged from the values of 0.25d wide region at axially 0.5d position, as indicated in the picture. Under the subcritical condition (pressure under 34 bar), the density of nitrogen showed a tendency of linearly increasing with rising chamber pressure condition. This is a reasonable result considering the equation of state (equation 3.1).

$$P = \rho RT \tag{3.1}$$

With assuming that the temperature condition is constant for each cases, it was expected for the increase in ambient pressure to result in higher fluid density value. This expectation well matched with the result under the subcritical pressure conditions, but not under the higher pressure conditions. Rather than

keep increasing, the density value of the injected nitrogen seemed to converge. Deeper consideration on this unexpected trend led to several hypotheses.

First hypothesis is that, under the supercritical condition, there is no surface tension on the supercritical fluid and it could have resulted in rapid diffusion. Rather than injected as a liquid nitrogen at the tip of the injector, nitrogen could have already changed into supercritical fluid inside the injector.

The second possible aspect is the signal attenuation occurring inside the jet stream. When a nitrogen molecule in the jet emits Raman scattering signal as being excited by the laser sheet, the intensity of the signal also attenuates as it passes through the other molecules surrounding the emitting source. Under the subcritical pressure conditions, relatively low density of liquid nitrogen jet could have affected the attenuation less than for the case of supercritical pressure conditions. This phenomena has possibility of resulting in nonlinear trend of density change under the supercritical pressure condition.

The third assumption takes the effect of specific heat value anomaly into account. Under the supercritical condition, fluid has liquid-like density but acts like vapor. There is no clear boundary between gas and liquid state, but still there is a region where the density changes rapidly with increasing temperature. This phenomena become to be investigated recently by Gorelli et al. [12], and Banuti and Hannemann [13] also took this phenomena into account while studying on the jet injection characteristic under supercritical conditions. Closer look into the thermophysical properties data provided by National Institute of Standards and Technology (NIST) also gives an insight to understand how the density of supercritical fluid would change with varying temperature [14].

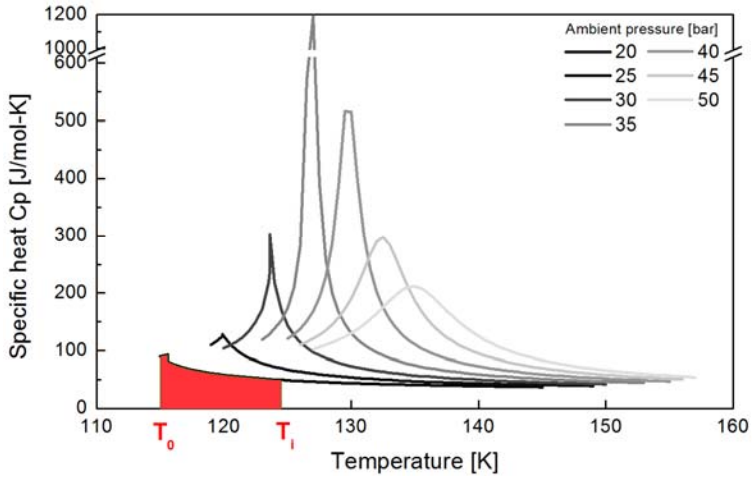

Figure 3.13 Specific heat value change of nitrogen flowing in the injector based on NIST data [14]

Figure 3.13 shows the change of specific heat value following the temperature change of the injected liquid nitrogen under different ambient pressure conditions. For each lines in the graph, the leftmost point is the property of liquid nitrogen inside the injector (T_0), based on the measured pressure and temperature value. As liquid nitrogen flows through the injector, it exchanges heat with injector wall, which would result in heat influx and temperature increase. Depending on where the maximum specific heat point is located, the same heat influx could have resulted in different final temperature (T_i) which is obtained by injected nitrogen fluid. In this study, the measurement of the injected nitrogen temperature was not able to be conducted, but taking this thermophysical characteristic into account would help to explain the trend of injection density decrease under the supercritical condition.

3.4 Normalized distribution analysis

In addition to density quantification of liquid nitrogen jet, normalized density analysis was carried on to compare the density distribution relative to the property at the injector tip, or the most-dense part, at each cases. The normalizing equation is given in equation 3.2,

$$Normalized\ density = \frac{\rho(\xi) - \rho_R}{\rho_I - \rho_R} \tag{3.2}$$

where ρ is density, ξ is normalized position given in equation 3.3, and subscript R and I stand for averaged background and maximum density part, respectively.

$$\xi = \frac{Axial\ position}{Injector\ diameter} \tag{3.3}$$

3.4.1 Axial normalization

The normalized density distribution along the center line of the injected nitrogen jet has been analyzed with the density data of the region indicated in figure 3.14

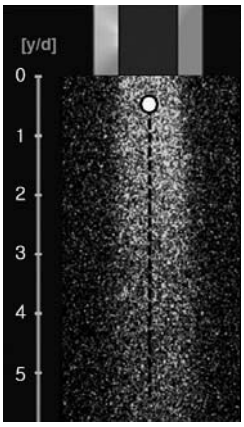

Figure 3.14 A region used for axial normalization analysis

The density value at the white circle (0.5d position from the injector tip) in figure 3.14 was used as the maximum density value for the normalization, $\boldsymbol{\rho_I}$. From axially 0.5d to 5.5d, the density values of each position were normalized and graphed in figure 3.15 and 3.16.

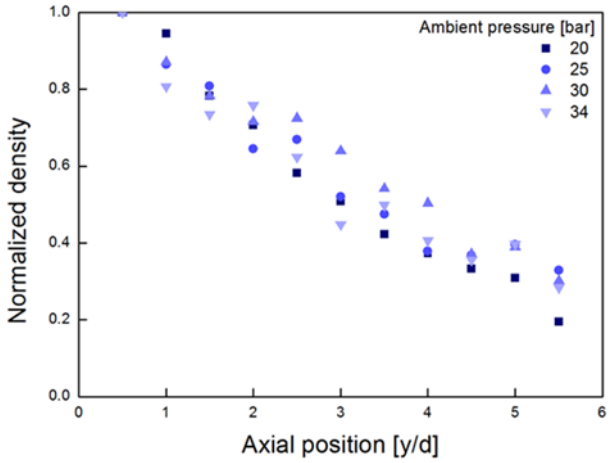

Figure 3.15 Axially normalized density distribution under subcritical and critical conditions

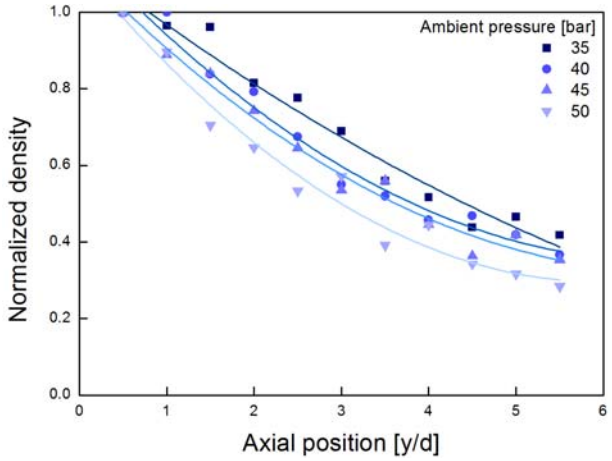

Figure 3.16 Axially normalized density distribution under supercritical conditions

From figure 3.15 and 3.16, the density of nitrogen jet along the center line decreases as the jet flows, which is natural. Comparing each experiment cases with others, there is no clear tendency of density-decreasing rate under the subcritical and critical pressure conditions (figure 3.15). However, under the supercritical pressure conditions, the speed of density decrease, when nitrogen jet flows, tends to be faster as the ambient pressure increases, as drawn in figure 3.16. This result states that, under the supercritical condition, the dissipation of the density is more aggressive as the ambient pressure increases. Even though it's the initial region of the jet injection, the density of nitrogen jet has been dissipated into less than 50 % of its initial value.

3.4.2 Radial normalization

In addition to the axial normalization, which showed a tendency of density dissipation rate along the center line of the nitrogen jet, a radial normalization analysis also has been carried on for a similarity study. To compare the similarity curve with previous research cases, the normalization process was slightly more complex than equation 3.2. At each axial positions and pressure conditions, the density value at the central part was set as $\boldsymbol{\rho_I}$ in equation 3.2. While normalizing density values according to equation 3.2, x-axis was re-scaled at the same time with setting the half-maximum position as R0.5 [11].

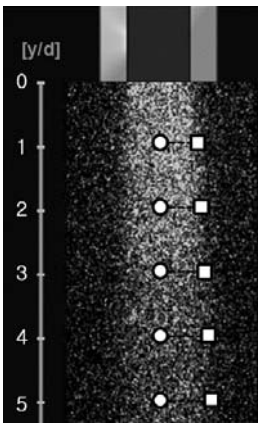

Figure 3.17 A region used for radial normalization analysis

Figure 3.17 has been attached to help understanding the region used for the normalization. The density values at the white circles are $\boldsymbol{\rho_I}$ values for each axial position cases. The white squares are locates where the density value falls to half of the central part, and this location becomes R0.5. The result graphs of the radial normalization are shown in figure 3.18, 3.19, and 3.20.

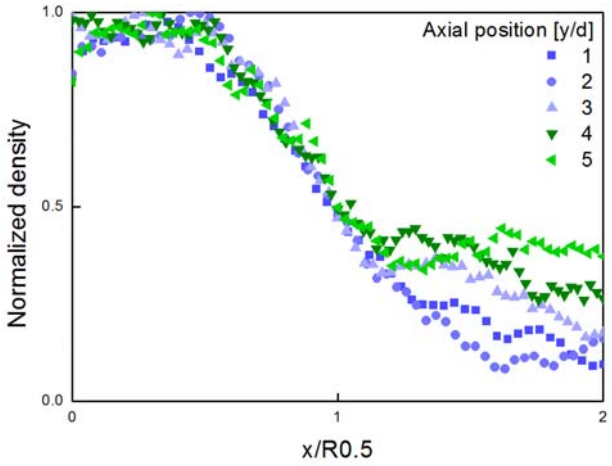

Figure 3.18 Radially normalized density distribution under subcritical condition (25 bar)

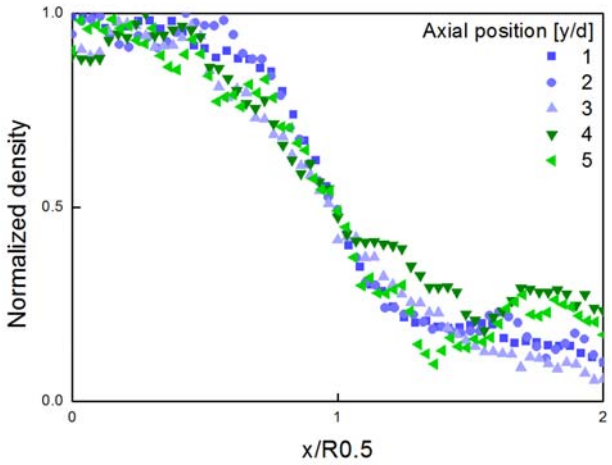

Figure 3.19 Radially normalized density distribution under critical condition (34 bar)

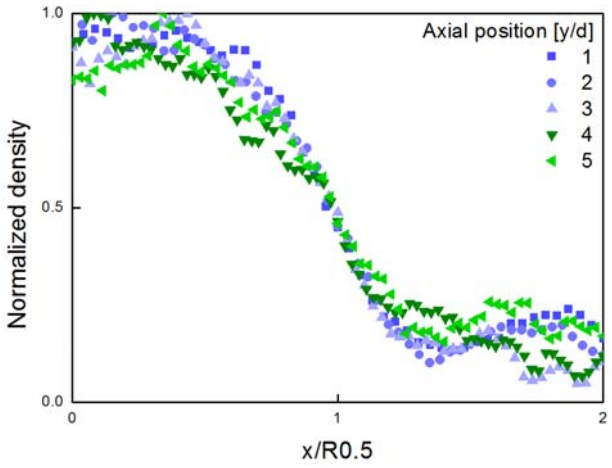

Figure 3.20 Radially normalized density distribution under supercritical condition (45 bar)

From the result of figure 3.18, 3.19, and 3.20, density distribution at axial position of 1d shows the similar shape regardless of the ambient pressure conditions. However, at 5d position, the density distribution shape differs from each other depending on the ambient pressure conditions. Under the subcritical conditions (figure 3.18), the similarity of the density distribution is not much preserved as the jet flows. On the other hand, under the supercritical condition (figure 3.20), there is no big deviation between the shape of density distribution at axial position of 1d and 5d.

Together with the result of axial normalization analysis, it could be concluded that, under the supercritical condition, the density of nitrogen decreases faster along the axial direction as pressure increases, but the similarity of the jet is better preserved than the subcritical conditions. Also taking the existence of

nitrogen droplets under the subcritical conditions into account, the better preservation of the similarity under the supercritical conditions could have resulted from its abnormal characteristic of supercritical fluid.

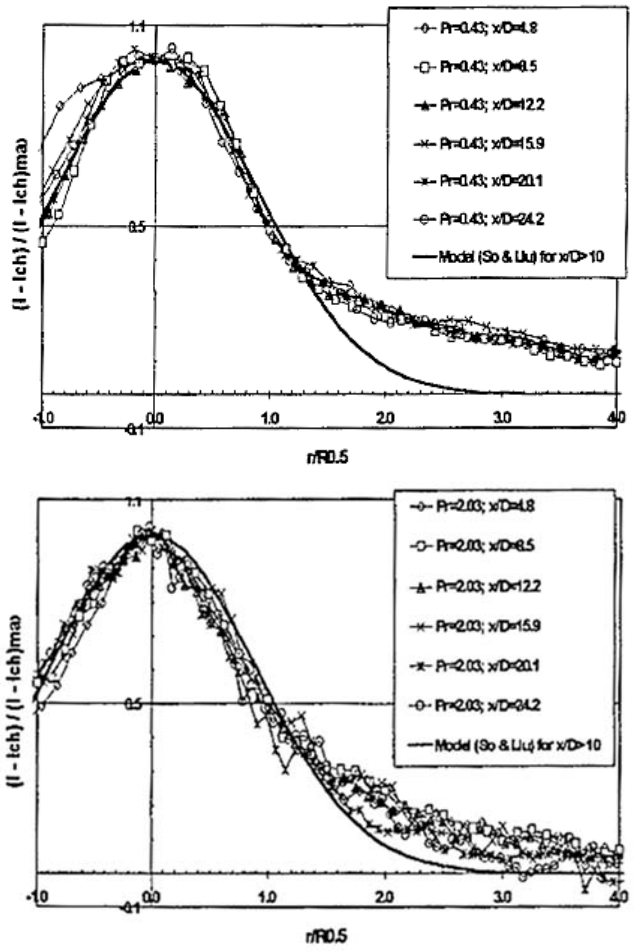

Figure 3.21 Similarity-type plot for the measured Raman intensity surplus (I-Ich) at sub- (above) and supercritical (below) chamber conditions. R0.5 is the radius at which (I-Ich) drops to half of its maximum [11]

To compare the result with previous study, the graphs of Chehroudi et al. [11] have been referred and attached in figure 3.21. The result of Chehroudi et al. is consist of data at the axial position from 4.8d to 24.2d, which is farther downstream than the interested region of this study: 1d to 5d. Chehroudi et al. also referred the modeling result studied by So et al. [15] for the comparison. According to the result of Chehroudi et al., the similarity of nitrogen jet fits better to the modeling result under the supercritical condition, and larger deviation on the jet similarity was observed under the subcritical condition as nitrogen jet flows. Even though So et al. bound the applicability of the modeling result to the axial position farther than 10d, the result of Chehroudi et al. and this study in figure 3.18, 3.19, and 3.20 showed the agreement even for the closer region.

3.5 Ramanographs

Since 1969, many efforts to apply Raman scattering principle to a gas flow investigation have been made by Sandia laboratories, and finally Hartley succeeded to map the 2-dimensional concentration in 1974 [16]. He named the technique as ‘Ramanography’ and the acquired 2-dimensional data set was called as ‘Ramanograph’. Ramanograph has advantages on analyzing the flow characteristics with a glance, because the density distribution and the value is indicated with color difference.

In addition to the sectional and normalized analysis of the nitrogen jet density distribution, Ramanographs were drawn and presented as figure 3.22 and 3.23. For the cases under subcritical conditions, vapor and liquid nitrogen coexist in the flow. Therefore, based on the color it shows, the phase of the nitrogen fluid inside the jet can be determined with the thermophysical properties given at each conditions. On the other hand, under the supercritical condition, there is no clear classification between liquid and vapor, but still, the density distribution of the nitrogen jet can be analyzed easily. For a comparison, unfiltered images of laser-scattered signals have been depicted using DSLR camera and those are presented in figure 3.24 and 3.25.

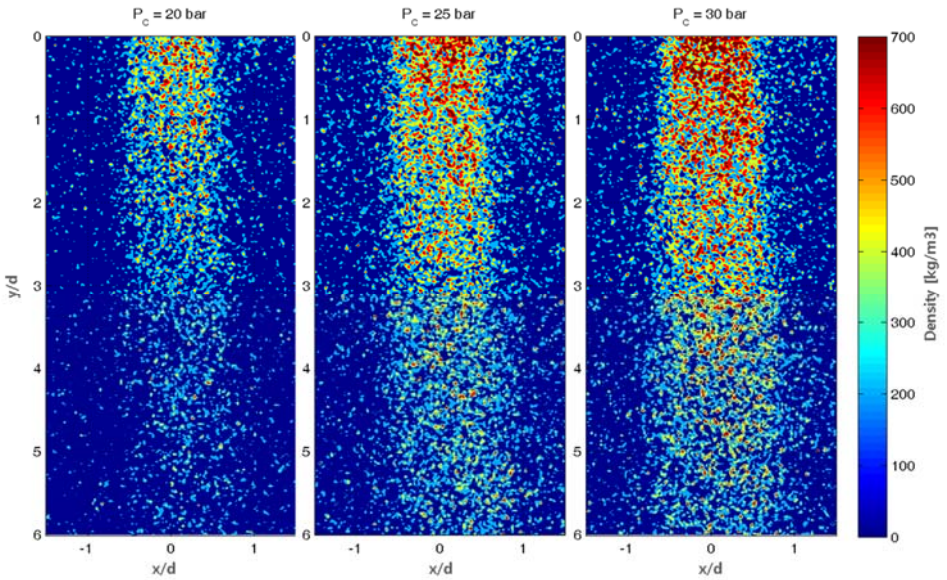

Figure 3.22 Ramanographs of nitrogen jet under subcritical conditions

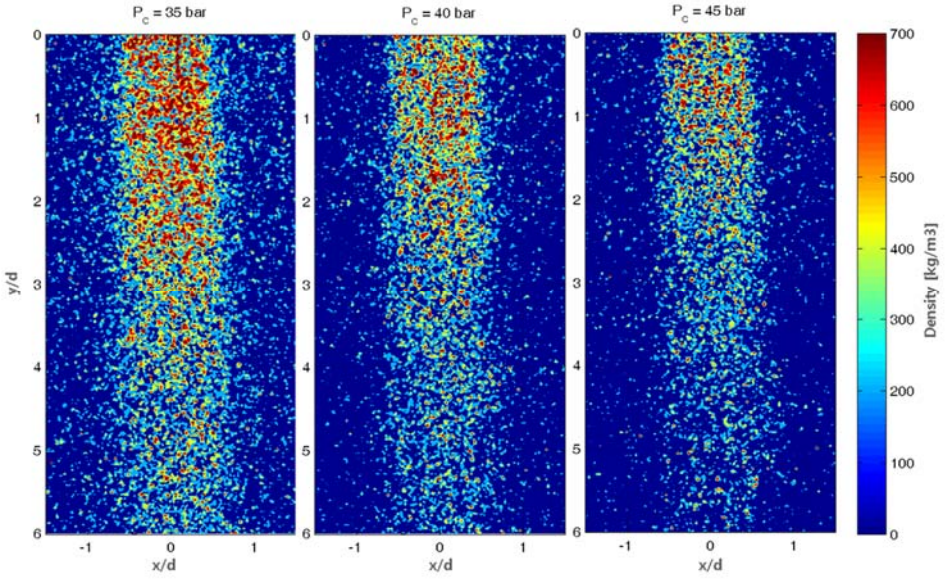

Figure 3.23 Ramanographs of nitrogen jet under supercritical conditions

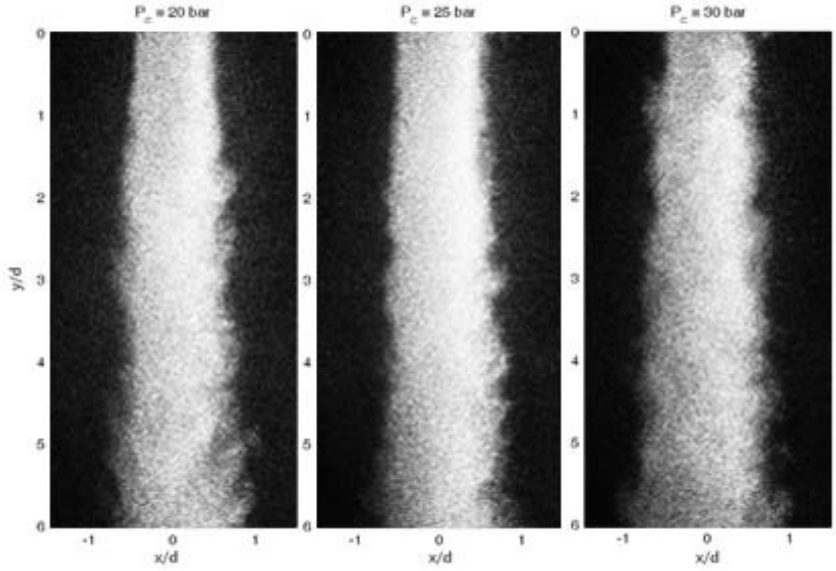

Figure 3.24 Unfiltered image of laser-scattered nitrogen injection under subcritical conditions

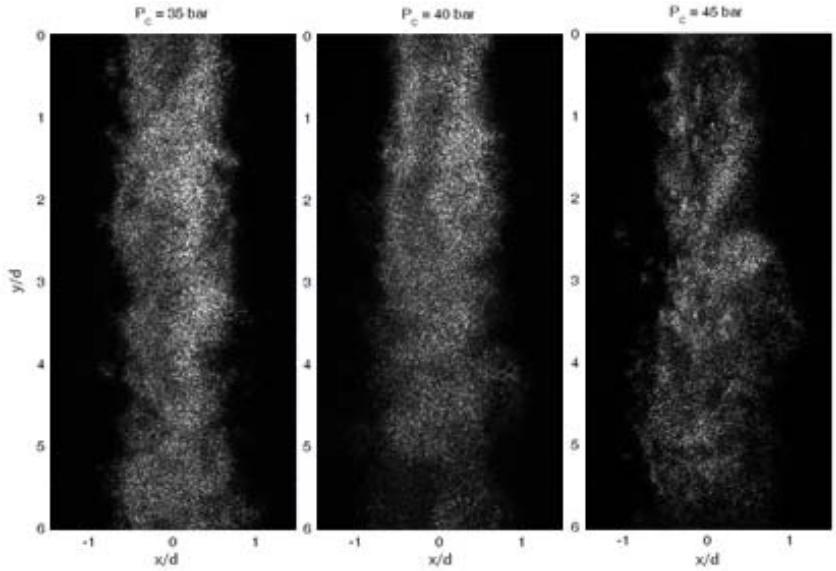

Figure 3.25 Unfiltered image of laser-scattered nitrogen injection under supercritical conditions

The major difference between the unfiltered image and the Raman scattering signal can be observed under the supercritical conditions. As the major portion of unfiltered scattering signal is Mie's scattering and refracted light, the signal intensity is stronger under the subcritical conditions due to the existence of droplets. However, under the supercritical conditions, the unfiltered signal becomes weaker even though the density of the flow is still large enough. Therefore, Ramanography would be a proper technique for a density distribution investigation, and direct photography method could be applied in different condition depending on the objectives of the study.

Chapter 4 CONCLUSION

In this study, Raman scattering technique has been applied to investigate cryogenic liquid nitrogen jet under various pressure conditions. Liquid nitrogen has been used instead of cryogenic propellant such as liquid oxygen, and high pressure chamber has been used for simulating the real rocket combustion chamber conditions. Before the high pressure chamber experiment, Raman scattering signal verification process was required in order to confirm the proper filter set which would perfectly block the incident beam wavelength and passes the Raman signal. At the same time, the power of laser was limited not to induce the break down phenomena which causes plasma formation.

In the high pressure chamber experiment, with a criterion of 34 bar which is nitrogen's critical pressure, the ambient pressure conditions were set as from 20 bar to 50 bar with the gap of 5 bar. Raman scattering signal images of the nitrogen injection were captured by ICCD camera, and the image went through several data reduction process to correct the distortion arose from background noise, Gaussian beam profile of the laser beam, and the beam attenuation inside the chamber. The refined data was quantified into a density map based on the relation between Raman signal intensity and density.

The density map of nitrogen jet under the various pressure conditions showed its distribution after the injector. Also a trend of nitrogen jet density was observed with changing ambient pressure conditions. Several hypotheses to understand the trend have been raised, but deeper research would be required to explain the phenomena in more detail.

A normalized density distribution also has been analyzed to observe the trend of density dissipation along the axis and the similarity conservation in its radial direction. The axial normalization showed no specific trend of dissipation rate under the subcritical conditions, but under the supercritical conditions, there was a clear tendency of faster decrease in density along the axis as the ambient pressure increases. The radial normalization analysis also had a meaning of studying the flow similarity conservation. Even though this research focused only on the initial region of the injection, a trend of better conservation of the similarity under the supercritical conditions well matched with the previous result cases, which focused more on the farther region of the injection.

At last, to understand the density distribution of the nitrogen jet easily, Ramanographs were drawn based on the images which went through a series of the data reduction process. Comparing the Ramanographs with the unfiltered laser-scattered image, the advantage of Raman scattering technique for quantifying the flow density was magnified, especially under harsh conditions such as high pressure and low temperature.

Based on this research, some parts could be studied in more detail related to this result or independently. One of those is the unnatural trend of the injected nitrogen density which converged into a certain value under the supercritical condition. A closer look into the equation 1.3 and the physics of a term, Raman scattering cross section, seems to be helpful to investigate the phenomena in more detail. In addition, this technique also has a potential to be used for a dynamics study of injection under the supercritical condition if it’s combined with cutting-edge equipment recently more affordable to researchers.

Bibliography

[1] G. P. Sutton and O. Biblarz, *Rocket propulsion elements*: John Wiley & Sons, 2010.

[2] S. Cho, G. Park, Y. Chung, Y. Yoon, and V. G. Bazarov, "Surface Instability on Cryogenic Swirl Flow at Sub- to Supercritical Conditions," *Journal of Propulsion and Power,* vol. 30, pp. 1038-1046, Jul-Aug 2014.

[3] M. Oschwald and A. Schik, "Supercritical nitrogen free jet investigated by spontaneous Raman scattering," *Experiments in Fluids*, vol. 27, pp. 497-506, Nov 1999.

[4] W. Mayer, J. Telaar, R. Branam, G. Schneider, and J. Hussong, "Raman measurements of cryogenic injection at supercritical pressure," *Heat and Mass Transfer,* vol. 39, pp. 709-719, Sep 2003.

[5] R. D. Woodward and D. G. Talley, "Raman imaging of transcritical cryogenic propellants," *AIAA paper,* vol. 468, 1996.

[6] B. Chehroudi, R. Cohn, and D. Talley, "Cryogenic shear layers: experiments and phenomenological modeling of the initial growth rate under subcritical and supercritical conditions," *International Journal of Heat and Fluid Flow,* vol. 23, pp. 554-563, Oct 2002.

[7] C. V. Raman, "A new radiation," *Indian Journal of physics,* vol. 2, pp. 387-398, 1928.

[8] W. R. Fenner, H. A. Hyatt, J. M. Kellam, and S. Porto, "Raman cross section of some simple gases," *Journal of the Optical Society of America,* vol. 63, pp. 73-77, 1973.

[9] H. Schlichting, K. Gersten, and K. Gersten, *Boundary-layer theory*: Springer Science & Business Media, 2000.

[10] M. Oschwald, A. Schik, M. Klar, and W. Mayer, "Investigation of coaxial LN2/GH2-injection at supercritical pressure by spontaneous Raman scattering,"

in *Proceedings of the 35th AIAA/ASME/SAE/ASEE Joint Propulsion Conference and Exhibit*, 1999.

[11] B. Chehroudi, R. Cohn, D. Talley, and A. Badakhshan, "Raman Scattering Measurement in the Initial Region of Sub-and Supercritical Jets," DTIC Document, 2000.

[12] F. Gorelli, M. Santoro, T. Scopigno, M. Krisch, and G. Ruocco, "Liquidlike behavior of supercritical fluids," *Physical review letters*, vol. 97, pp. 245-702, 2006.

[13] D. T. Banuti and K. Hannemann, "Supercritical Pseudo-Boiling and its Relevance for Transcritical Injection," in *50th AIAA/ASME/SAE/ASEE Joint Propulsion Conference*, 2014.

[14] R. Span, E. W. Lemmon, R. T. Jacobsen, W. Wagner, and A. Yokozeki, "A reference equation of state for the thermodynamic properties of nitrogen for temperatures from 63.151 to 1000 K and pressures to 2200 MPa," *Journal of Physical and Chemical Reference Data*, vol. 29, pp. 1361-1433, 2000.

[15] R. So, J. Zhu, M. Ötügen, and B. Hwang, "Some measurements in a binary gas jet," *Experiments in Fluids*, vol. 9, pp. 273-284, 1990.

[16] D. L. Hartley, "Raman gas mixing measurements and Ramanography," in *Laser Raman Gas Diagnostics*, ed: Springer, pp. 311-314, 1974.

[17] W. Mayer, A. Schik, C. Schweitzer, and M. Schaffler, "Injection and mixing processes in high pressure LOX/GH2 rocket combustors," *AIAA paper*, pp. 1-3, 1996.

[18] H. Sponer, "Absorption Bands in Nitrogen," *Proceedings of the National Academy of Sciences of the United States of America*, vol. 13, p. 100, 1927.

[19] H. A. Szymanski, *Raman spectroscopy: theory and practice* vol. 2: Plenum Press, 1970.

[20] M. Lapp and C. M. Penney, *Laser Raman gas diagnostics*: Springer, 1974.

[21] A. Lofthus and P. H. Krupenie, "The spectrum of molecular nitrogen," *Journal of physical and chemical reference Data*, vol. 6, pp. 113-307, 1977.

[22] A. Rotem and S. Rosenwaks, "Laser-induced fluorescence studies of molecular

nitrogen," *Optical Engineering*, vol. 22, pp. 225564-225564-, 1983.

[23] M. Decker, A. Schik, U. E. Meier, and W. Stricker, "Quantitative Raman imaging investigations of mixing phenomena in high-pressure cryogenic jets," *Applied optics*, vol. 37, pp. 5620-5627, 1998.

[24] B. Chehroudi, D. Talley, and E. Coy, "Fractal geometry and growth rate changes of cryogenic jets near the critical point," in *50th AIAA/ASME/SAE/ASEE Joint Propulsion Conference*, Los Angeles, California, 1999.

[25] B. Chehroudi, D. Davis, J. Graham, A. Karagozian, I. Leyva, J. Rodriguez, *et al.*, "Dynamics of Supercritical Flows," DTIC Document, 2012.

[26] G. C. Herring and B. Shirinzadeh, *Flow Visualization of Density in a Cryogenic Wind Tunnel Using Planar Rayleigh and Raman Scattering*: NASA Langley Research Center, 2002.

[27] B. Chehroudi, "Recent experimental efforts on high-pressure supercritical injection for liquid rockets and their implications," *International Journal of Aerospace Engineering*, 2012.

초 록

본 연구에서는 실제 로켓 엔진 연소기의 조건을 모사한 분사 특성 분석이 진행되었다. 액체질소를 작동 유체로 이용함으로써 극저온 로켓 추진제를 모사하였고, 분사 실험은 고압 챔버 내부에서 진행함으로써 다양한 압력 조건을 형성할 수 있도록 하였다. 극저온 유동 가시화의 짧은 촬영 가능시간 문제를 해결하기 위해 레이저를 이용한 라만 산란 기법을 적용하였고, 이로써 정량적 분석 또한 가능하였다. 라만 산란의 발생 여부와 적절한 필터의 조합은 고압 챔버 실험에 앞서 확인 및 검증되었다. 필터군은 조사광 파장대의 빛을 10^{-16} 수준으로 차단할 수 있도록 조합되었다. 붕괴 (breakdown) 현상을 유도하는 레이저의 출력 범위를 측정하였고, 이 기준에 따라 플라즈마가 형성되지 않는 최대값으로 출력을 설정하였다.

고압 챔버 실험에서의 주위 기체 압력 조건은 질소의 아임계 조건에서 초임계 조건까지인 20 bar에서 50 bar까지로 설정되었다. 질소 제트에 의해 발생된 라만 산란 신호는 ICCD 카메라를 이용하여 기록되었고, 이 이미지는 배경 노이즈 제거, 가우시안 빔 분포 영향 보정, 조사광 감쇠 영향 보정 과정을 거쳤다. 보정된 이미지는 밀도장으로 정량화되었고 다양한 관점에서 분석되었다.

밀도장 데이터를 통해 분사된 질소 제트의 밀도 분포를 그 값으로 확인할 수 있었다. 또한, 축 방향 0.5d 위치에서의 밀도 변화를 분석함으로써 주위 기체 압력 조건 변화에 따른 분사 유체 밀도 변화의 경향성을 확인할 수 있었다. 이 결과, 아임계 조건에서는 압력이 증가함에 따라 유체 밀도 또한 증가하는 경향을 보였으나, 초임계 조건에서는 압력 증가와 무관하게 밀도 값이 수렴하는 특성을 확인하였다. 밀도장 표준화를 통한 분석 또한 진행하였다. 축 방향으로 표준화한 데이터 분석을 통해 초임계 조건에서 압력이 증가할수록 유체의 진행에 따른 소산 정도가 큰 것을 확인할 수 있었다. 반경

방향으로 표준화한 데이터는 제트의 유사성 분석에 이용되었고, 아임계 조건에서 그 유사성 유지 정도가 감소하는 현상을 확인할 수 있었다. 밀도장 분석의 편이성을 위해 라마노그래프 또한 작성되었고, 필터링 되지 않은 제트 유동의 레이저 산란 이미지와 비교함으로써 라만 산란 기법의 적합성을 확인하였다.

주요어: 라만 산란, 레이저 계측, 제트 인젝터, 극저온, 초임계, 액체질소
학 번: 2013-23063